IEEE Access
Multidisciplinary | Rapid Review | Open Access Journal

Date of publication xxxx 00, 0000, date of current version xxxx 00, 0000.

Digital Object Identifier 10.1109/ACCESS.2020.DOI

Digital Predistortion of Millimeter-Wave Hybrid Beamforming Transmitters using Observation Receivers with Low-Bit Resolution Analog-to-Digital Converter

A. BEN AYED[1], (Student Member, IEEE), E. NG[2], (Student Member, IEEE), P. MITRAN[1], (Senior Member, IEEE), and S. BOUMAIZA[1], (Senior Member, IEEE)

[1]Department of Electrical and Computer Engineering, University of Waterloo, Waterloo, ON N2L 3G1, CA (e-mail: abenayed@uwaterloo.ca, pmitran@uwaterloo.ca, and sboumaiza@uwaterloo.ca)

[2]Anokiwave Inc., Billerica, MA 01821, USA (e-mail: eric.ng@anokiwave.com)

Corresponding author: A. BEN AYED (e-mail: abenayed@uwaterloo.ca).

ABSTRACT This paper proposes a new digital predistortion (DPD) scheme for linearizing millimeter-wave hybrid beamforming transmitters using observation receivers with low-bit resolution analog-to-digital converters (ADCs). To train the DPD function required to compensate for the distortions exhibited by a given sub-array (also called main sub-array), an error signal is produced by out-of-phase combining the main sub-array transmitted signal and the one generated by another sub-array (also called auxiliary sub-array) using anti-beamforming modules. The error signal is then frequency down-converted and digitized using a low-bit resolution ADC. Proof-of-concept validation experiments are conducted by applying the proposed DPD system to linearize an off-the-shelf hybrid-beamforming array comprised of four 64-element sub-arrays, operating at 28 GHz and driven with up to 800 MHz orthogonal frequency-division multiplexing modulated signals. Using the proposed DPD scheme, an observation receiver with a 4-bit ADC was sufficient to improve the adjacent channel power ratio by 10 dB and the error vector magnitude was reduced from 5.8% to 1.6%. These results are similar to those obtained using an observation receiver with 16-bit ADC.

INDEX TERMS Digital predistortion, hybrid beamforming, massive MIMO, millimeter-waves, nonlinear power amplifiers.

I. INTRODUCTION

LARGE scale multiple-antenna (LSMA) radio systems operating at millimeter-wave (mmwave) frequencies will be key technologies to meet the requirements of future wireless networks. The realization of viable mmwave LSMA radio hardware is very challenging, especially at the transmitter side where the trade-off between linearity and efficiency is of critical importance. Specifically, the underlying mmwave power amplifiers (PAs) suffer from notably lower efficiency when compared to their sub-6 GHz counterparts. In addition, they exhibit non-negligible non-linearity that significantly degrades their output signal quality. This issue is exacerbated when the PAs are driven with wide bandwidth modulated signals. Hence, the deployment of linearization techniques such as digital predistortion (DPD) is essential to maximize the trade-off between their linearity and efficiency.

Recently, attempts have been made to devise advanced DPD schemes tailored to LSMA front-ends operating at microwave or mmwave frequencies. These can be classified into two distinct categories: those that use multi-input (mainly dual-input) modelling approaches, and those based on single-input, single-output (SISO) modelling approaches. For instance, dual-input DPD schemes were proposed in [1]–[4] to linearize PAs in a 4-element digital beamforming LSMA operating at the sub-6 GHz band. Alternatively, lower complexity SISO DPD schemes have demonstrated interesting linearization capacity when applied to LSMA front-ends driven with 5G signals and operating at sub-6 GHz [5]–[10] or mmwave signals [11]–[16]. To train the underlying DPD functions, the above-mentioned schemes used feedback signals that were either (i) sampled at the PA outputs using dedicated transmitter observation receivers (TOR) [7], [10],

This article has been accepted for publication in a future issue of this journal, but has not been fully edited. Content may change prior to final publication. Citation information: DOI 10.1109/ACCESS.2021.3096978, IEEE Access

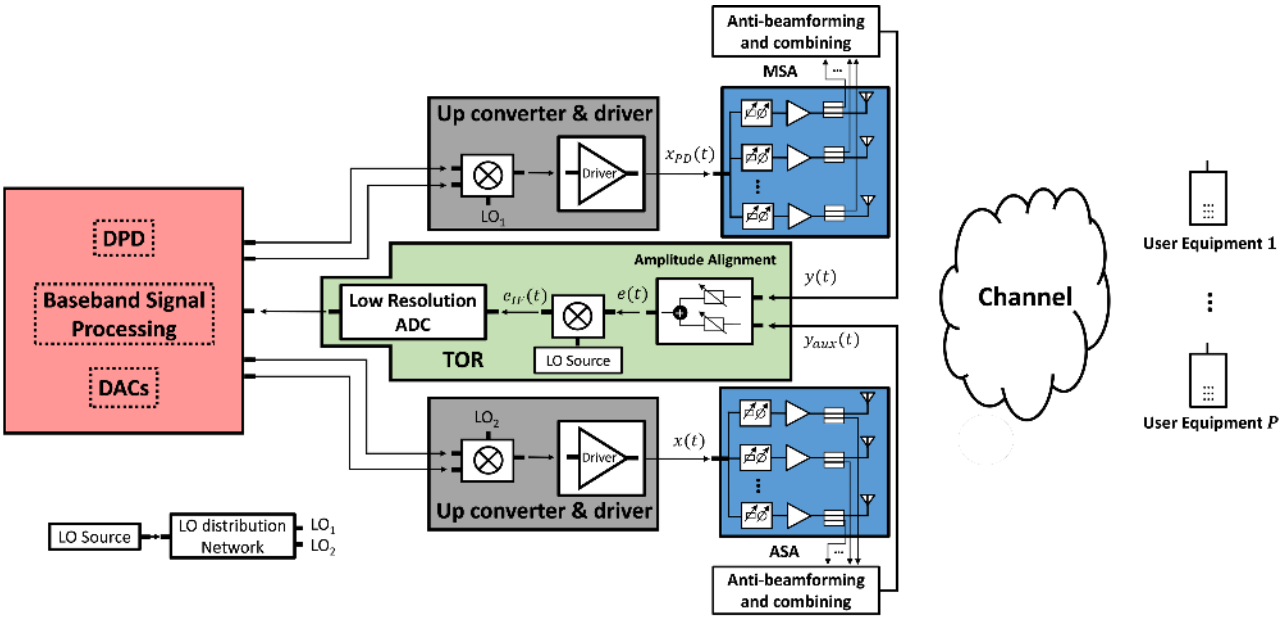

FIGURE 1. Block diagram of proposed DPD system for the case of a two sub-array hybrid beamformer: MSA transmits $x_{PD}(t)$; ASA transmits $x(t)$.

(ii) extracted using an anti-beamforming TOR module that generates a far-field equivalent signal [11], (iii) captured using a far-field probing antenna [7], [12], [17], or (iv) using near-field probing antennas [14]–[16].

The above-mentioned DPD schemes demonstrated promising linearization capacity. Nevertheless, it is critical to reduce the power overheads associated with the implementation of the DPD function, the TOR hardware and the training algorithm, especially as the signal bandwidth broadens to attain hundreds of MHz. While advancements in FPGA hardware [18] help to reduce the implementation burden of the DPD engine, the power consumption of the high-speed analog-to-digital converter (ADC) stage of the TOR remains a major challenge. This is because it requires both high bit-resolution (typically 8-14 bits) and Giga-samples-per-second (Gsps) sampling rate to cope with the spectrum regrowth due to the PA nonlinearity (up to 5-times the signal bandwidth). Such ADCs are costly in terms of power consumption, i.e., the ADC12J4000 is a 12 bits ADC that consumes 2 to 3 Watts when operated at 4 Gsps. Therefore, for DPD to provide an overall power benefit, it is critical to reduce the TOR power requirements. This includes, for example, decreasing the required ADC sampling rate and bit resolution.

Recently, several publications have reported new approaches to reducing the ADC sampling rate [7], [10], [19]–[21] at the cost of signal processing overhead. Nevertheless, reducing the required bit resolution has not seen significant research attention. In fact, only recently has a new DPD system been proposed in [22], [23] to reduce the required ADC bit resolution. For instance, in [22], the authors reduced the required dynamic range of the TOR and consequently the ADC resolution by sampling and capturing an error signal instead of the PA output signal. The error signal used in [22] is the difference between the input and output signals of the PA. Once sampled, the error signal is then used to digitally generate the PA output signal for DPD training. Experiments reported in [22] demonstrated a successful ADC resolution reduction from 12 bits to 8 bits using a test signal of 40 MHz bandwidth. Higher ADC bit resolution reduction was reported in [23], where a 1-bit complex TOR was used to train the DPD function. It is to note that both [22] and [23] are tailored to a single PA deployment and rely on the deployment of full additional transmitter chains to generate a copy of the PA input signal and ideal signal respectively.

In this paper, a novel SISO DPD scheme (illustrated in Fig. 1) is proposed to linearize a mmwave hybrid-beamforming based LSMA while using a TOR with low bit resolution ADCs. The paper is structured as follows. Section II outlines the newly proposed DPD scheme and describes its theoretical basis. Section II also highlights the underlying challenges associated with the proposed scheme practical implementation, namely local oscillator (LO) phase-offset and delay alignment. It also describes methods devised to tackle these challenges. Experimental results are presented in Section III and conclusions are summarized in Section IV.

A note on the notational style: In this paper, RF signals are denoted without a subscript while IF signals are denoted with the subscript IF—i.e., $x(t)$ is an RF signal and $x_{IF}(t)$ is the corresponding IF signal. The complex baseband envelope of $x(t)$ is denoted in the text as $\tilde{x}(t)$. The discrete-time representation of $x(t)$, $x_{IF}(t)$ and $\tilde{x}(t)$ are $x[n]$, $x_{IF}[n]$ and $\tilde{x}[n]$, respectively. In addition, $\tilde{\mathbf{x}}[n]$, denotes a block of M samples, such that $\tilde{\mathbf{x}}[n] = (\tilde{x}[n], \tilde{x}[n-1], ..., \tilde{x}[n-M+1])$. If $\tilde{x}[n]$ and $\tilde{h}[n]$ are two discrete time sequences, then

$(\tilde{\mathbf{h}} * \tilde{x})[n] = \sum_k \tilde{h}[k]\tilde{x}[n-k]$ denotes the convolution of the sequence $\tilde{h}[n]$ with $\tilde{x}[n]$. Finally, $(\tilde{\mathbf{h}} * \tilde{\mathbf{x}})[n]$ denotes the vector $(\tilde{z}[n], \tilde{z}[n-1], ..., \tilde{z}[n-M+1])$ where $\tilde{z}[n] = (\tilde{\mathbf{h}} * \tilde{x})[n]$.

II. OVERVIEW AND THEORETICAL FORMULATION OF PROPOSED SISO DPD SCHEME

Fig. 1 shows the high-level block diagram of the proposed SISO DPD scheme applied to a hybrid beamforming system with, for simplicity of exposition, two sub-arrays. The proposed scheme exploits the inherent modularity of the hybrid-beamforming system to minimize the hardware requirements of the TOR. In particular, the training of the DPD function for each sub-array is conducted separately using a weighted sum of the constituent sub-array outputs. We denote the sub-array to be linearized as the main sub-array (MSA); the second sub-array is referred to as the auxiliary sub-array (ASA). During the DPD training process, the MSA transmits a pre-distorted input $x_{PD}(t)$ of the desired RF signal $x(t)$, while the ASA transmits $x(t)$. In the following, the anti-beamforming module connected to the MSA allows for the generation of a weighted sum, $y(t)$, of the signals transmitted by the constituent MSA antennas. The output signal of the anti-beamforming module is equivalent to the signal received by a far-field antenna in the main beam's direction, and includes the distortions introduced by the PAs in the MSA. Similarly, the anti-beamforming module of the ASA generates an output signal denoted by $y_{aux}(t)$ which is an inverted replica of the ASA input signal, $x(t)$, i.e., $y_{aux}(t) = -x(t)$. To ensure proper cancellation of $x(t)$ in $y(t)$, and to generate the error (distortion) signal $e(t)$ that will be used for DPD training, two attenuators are used to adjust the magnitudes of $y(t)$ and $y_{aux}(t)$. To simplify the theoretical derivations of the proposed DPD scheme, the following expression of the error signal is written assuming proper amplitude alignment of $y(t)$ and $y_{aux}(t)$, such that

$$e(t) = y(t) + y_{aux}(t) \quad (1)$$
$$= y(t) - x(t), \quad (2)$$

The error signal is then down-converted to IF to obtain $e_{IF}(t)$, digitized using an ADC to obtain $e_{IF}[n]$, and further digitally down-converted to obtain the complex baseband signal $\tilde{e}[n]$. Fig. 2 shows an example of the MSA transmitted signal, $\tilde{y}(t)$, and the corresponding error signal, $\tilde{e}(t)$. In this case the input signal $\tilde{x}(t)$ is an 800 MHz orthogonal frequency-division multiplexing (OFDM) signal and the MSA and ASA are instances of a 64-element sub-array. Based on Fig. 2, the digitization of the IF error signal, $e_{IF}(t)$, would require an ADC with a lower bit resolution than that of the ADC to sample $y_{IF}(t)$.

Note, the proposed DPD scheme aims to exploit the already existing sub-arrays in hybrid beamforming systems to reduce the ADC bit resolution in the TOR needed to train the DPD functions and linearize the different sub-arrays. In the proposed DPD scheme of Fig. 1, during DPD training, the non-linear MSA transmits a signal at full power from which the error signal will be extracted. Two cases can be encountered:

- Case 1: the ASA used to extract the error signal is already linearized and its corresponding users will still be served while the DPD training for the MSA is ongoing. Using the proposed scheme depicted in the Fig. 1, the ASA transmits $x(t)$, the intended signal to its user. The ASA anti-beamforming module is used to coherently combine the ASA PAs output signals with an $180°$ phase-offset such that the ASA anti-beamformer output signal is $y_{aux}(t) = -x(t)$. The ASA and MSA anti-beamformers outputs are then combined to generate the error signal to train the DPD function and linearize the MSA using an ADC with reduced bit resolution. During this training phase, the MSA transmits the same signal as the ASA while directing its beam away from the ASA user to avoid interference. Note, the ASA beamformer setting (phases) do not need to be adjusted for maximum cancellation with the MSA outputs. In fact, the cancellation is ensured by the phase shift in the anti-beamforming modules [9].

- Case 2: the ASA used to extract the error signal is not linearized. In this case the ASA must be operated in backoff, with temporary reduced coverage range, to avoid non-linear distortions. During the training phase, the MSA transmits at full power the same signal as the ASA used to generate the error signal. In order to ensure proper cancellation of $x(t)$ from $y(t)$ the attenuators shown in Fig. 1 are used to adjust the magnitudes of $y(t)$ and $y_{aux}(t)$.

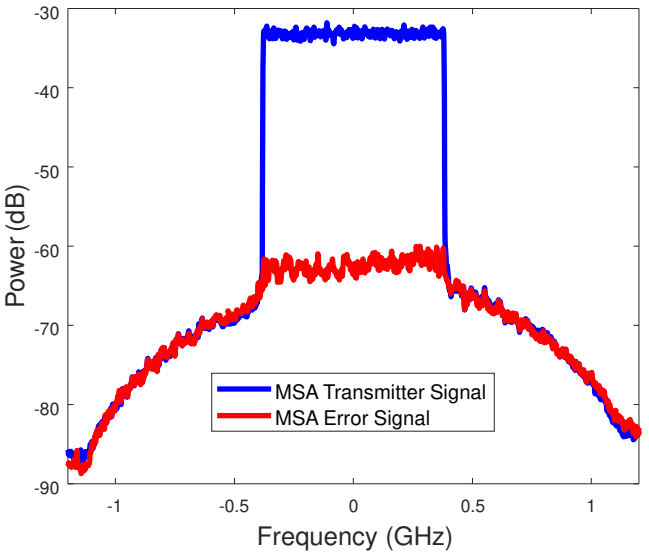

FIGURE 2. Power spectral density of the MSA transmitted signal, $\tilde{y}(t)$, and corresponding non-linear error signal $\tilde{e}(t)$.

A. DPD FORMULATION

Prior works in [5]–[17], [24], [25] demonstrated that a SISO DPD scheme is effective for linearizing LSMA front-ends of beamforming arrays. Various behavioral models can be used to describe the relationship between the input of an antenna

sub-array and the far-field signal or its equivalent $y(t)$, obtained using an anti-beamforming module. In this paper, the Complexity-Reduced Volterra model (CRV) outlined in [26] is used as the DPD model. Accordingly, the sampled complex envelope pre-distorted signal, $\tilde{x}_{PD}[n]$, is expressed as

$$\begin{aligned}\tilde{x}_{PD}[n] &= \sum_{\substack{i=0\\even}}^{N} \kappa_i \tilde{d}[n]\left|\tilde{d}[n]\right|^i + \sum_{m=1}^{M_L} \dot{\kappa}_m \tilde{d}[n-m] \\ &+ \sum_{\substack{i=1\\odd}}^{N}\sum_{m=1}^{M_{NL}}\sum_{\substack{j=2\\even}}^{N} \dot{\eta}_{i,m,j}\tilde{d}[n]\left|\tilde{d}[n]\right|^{i-1}\left|\tilde{d}[n-m]\right|^j \\ &+ \sum_{\substack{i=2\\even}}^{N}\sum_{m=1}^{M_{NL}}\sum_{\substack{j=1\\odd}}^{N} \ddot{\eta}_{i,m,j}\left|\tilde{d}[n]\right|^i\tilde{d}[n-m]\left|\tilde{d}[n-m]\right|^{j-1},\end{aligned} \tag{3}$$

where, N denotes the nonlinearity order, M_L denotes the linear memory depth, M_{NL} denotes the nonlinear memory depth, and the model coefficients are denoted by $\{\kappa_i, \dot{\kappa}_m, \dot{\eta}_{i,m,j}, \ddot{\eta}_{i,m,j}\}$. The nonlinear memory of the higher order terms are pruned following the procedure in [27], such that the nonlinear memory basis functions are limited to those satisfying the condition $i+m+j \leq N$. Alternatively, (3) can be rewritten as follows,

$$\tilde{x}_{PD}[n] = \sum_{l=1}^{L} a_l \psi_l(\tilde{\mathbf{x}}[n]), \tag{4}$$

where L is the total number of DPD bases and a_l is the l^{th} DPD coefficient. Here, without loss of generality, the first basis function $\psi_1(\tilde{\mathbf{x}}[n])$ is taken to be

$$\psi_1(\tilde{\mathbf{x}}[n]) = \tilde{x}[n]. \tag{5}$$

To apply the DPD model given by (3) and (4), first the underlying coefficients $\mathbf{a} = (a_1, ..., a_L) \in \mathbb{C}^L$ must be identified. In this work, the direct learning approach, described previously in [21], [28], is adopted whereby blocks of the baseband input $\tilde{x}[n]$ and corresponding error $\tilde{e}[n] = \tilde{y}[n] - \tilde{x}[n]$ are used to iteratively refine the estimate of $\mathbf{a}$. This yields a sequence $\mathbf{a}^{(1)}, \mathbf{a}^{(2)}, ..., \mathbf{a}^{(N)}$ of estimates of the predistorter coefficients. In the experimental results presented in Section IV, we take the predistorter coefficients, $\mathbf{a}$, to be the last of such estimates, i.e., $\mathbf{a} = \mathbf{a}^{(N)}$. Specifically, before the 1st iteration the predistorter is chosen to pass $\tilde{x}[n]$ undistorted, i.e.,

$$\mathbf{a}^{(1)} = (1, 0, ..., 0), \tag{6}$$

and the coefficients after the ℓ^{th} iteration, $1 \leq \ell \leq N-1$, are updated according to

$$\mathbf{a}^{(\ell+1)} = \mathbf{a}^{(\ell)} - \gamma_\ell \Delta\mathbf{a}^{(\ell)}, \tag{7}$$

where $0 < \gamma_\ell < 1$ is the update step size at iteration ℓ, and $\Delta\mathbf{a}^{(\ell)} \in \mathbb{C}^L$ is the update direction of the predistorter model coefficients obtained using the following update equation,

$$\Delta\mathbf{a}^{(\ell)} = \left((\Psi^{(\ell)})^H \Psi^{(\ell)}\right)^{-1} (\Psi^{(\ell)})^H \tilde{\mathbf{e}}^{(\ell)}, \tag{8}$$

where

$$\tilde{\mathbf{e}}^{(\ell)} = (\tilde{e}[n_\ell], ..., \tilde{e}[n_\ell + M - 1])^T, \tag{9}$$

M is the total number of samples used to train the DPD function and $\tilde{e}[n_\ell]$ is the ℓ^{th} iteration non-linear error corresponding to sample indexed n_ℓ.

Hence, together (3), (6), (7), and (8) comprise the iterative training process that identifies the predistortion coefficients. As suggested in [10] and [12], the previously described training process should be conducted for a selection of steering angles to account for the steering angle dependent load modulation exhibited by RF arrays with non-ideal coupling.

B. TIME DELAY AND LO PHASE-OFFSET CALIBRATION

In the hybrid beamforming architecture illustrated in Fig. 1, the determination of the delay and phase offset between the MSA and ASA is critical to enable DPD training using an ADC with low bit resolution while maintaining good linearization capacity.

In order to identify both the phase-offsets ϕ_k of the different LO inputs and the time delays t_d^k at the different RF paths, the cross-correlation method in [29] is used. To that end, two complex signals, $x_k(t)$, $k = 1, ..., K = 2$, are generated to feed the two sub-arrays. Note, in this sub-section, both the MSA and ASA are operated in backoff.

Let $C_{\tilde{x}_k\tilde{x}_{\bar{k}}}(\tau)$ be the cross-correlation between $\tilde{x}_k(t)$ and $\tilde{x}_{\bar{k}}(t)$, defined by

$$C_{\tilde{x}_k\tilde{x}_{\bar{k}}}(\tau) = \int_{-\infty}^{+\infty} \tilde{x}_k(t) \times \tilde{x}_{\bar{k}}^*(t-\tau)dt. \tag{10}$$

The signals $\tilde{x}_k(t), k = 1, ..., K = 2$, are chosen such that:

1) The cross-correlation $C_{\tilde{x}_k\tilde{x}_{\bar{k}}}(\tau)$ is small $\forall\tau$ and $k \neq \bar{k}$

2) The auto-correlation $C_{\tilde{x}_k\tilde{x}_k}(\tau)$ has a large positive real-value for $\tau = 0$, and decays quickly for $|\tau| > 0$. The complex baseband signals $\tilde{x}_k(t), k = 1, ..., K = 2$, are generated in the discrete domain using multi-tones with random phases and magnitudes. The combined complex baseband output at the TOR, $\tilde{z}(t)$, can be written as

$$\tilde{z}(t) = \sum_{k=1}^{K} G_k \tilde{x}_k(t - t_d^k) e^{-j(\phi_k + \phi_0)}, \tag{11}$$

where ϕ_0 is the phase-offset introduced by the down-converting mixer and G_k is the k^{th} sub-array gain. From (10) and (11), the cross-correlation coefficients between the received signal $\tilde{z}(t)$ and the k^{th} input signal, $\tilde{x}(t)$, can be computed as,

$$\begin{aligned} C_{\tilde{x}_k\tilde{z}}(\tau) &= \int_{-\infty}^{+\infty} \tilde{x}_k(t) \times \tilde{z}^*(t-\tau)dt \qquad (12)\\ &= C_{\tilde{x}_k\tilde{x}_k}(\tau + t_d^k) \times G_k e^{j(\phi_k+\phi_0)} \\ &\quad + \sum_{\bar{k}\neq k} C_{\tilde{x}_k\tilde{x}_{\bar{k}}}(\tau + t_d^{\bar{k}}) \times G_{\bar{k}} e^{j(\phi_{\bar{k}}+\phi_0)}. \qquad (13)\end{aligned}$$

Given that the cross-correlation between different input signals $C_{\tilde{x}_k\tilde{x}_{\bar{k}}}(\tau)$, $k \neq \bar{k}$ is small, (13) can be approximated as

$$C_{\tilde{x}_k\tilde{z}}(\tau) \cong C_{\tilde{x}_k\tilde{x}_k}(\tau + t_d^k) \times G_k e^{j(\phi_k+\phi_0)}. \tag{14}$$

This article has been accepted for publication in a future issue of this journal, but has not been fully edited. Content may change prior to final publication. Citation information: DOI 10.1109/ACCESS.2021.3096978, IEEE Access

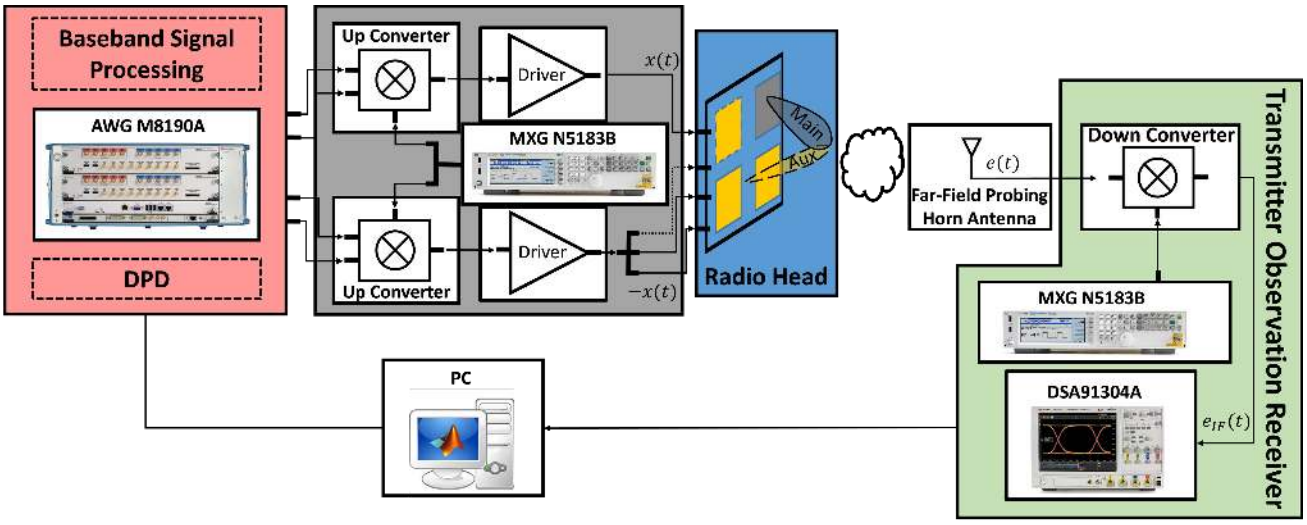

FIGURE 3. Block diagram of experimental setup with two alternate configurations of the radio head: three ASAs (see sub-section III-B), and two ASAs (see sub-section III-C).

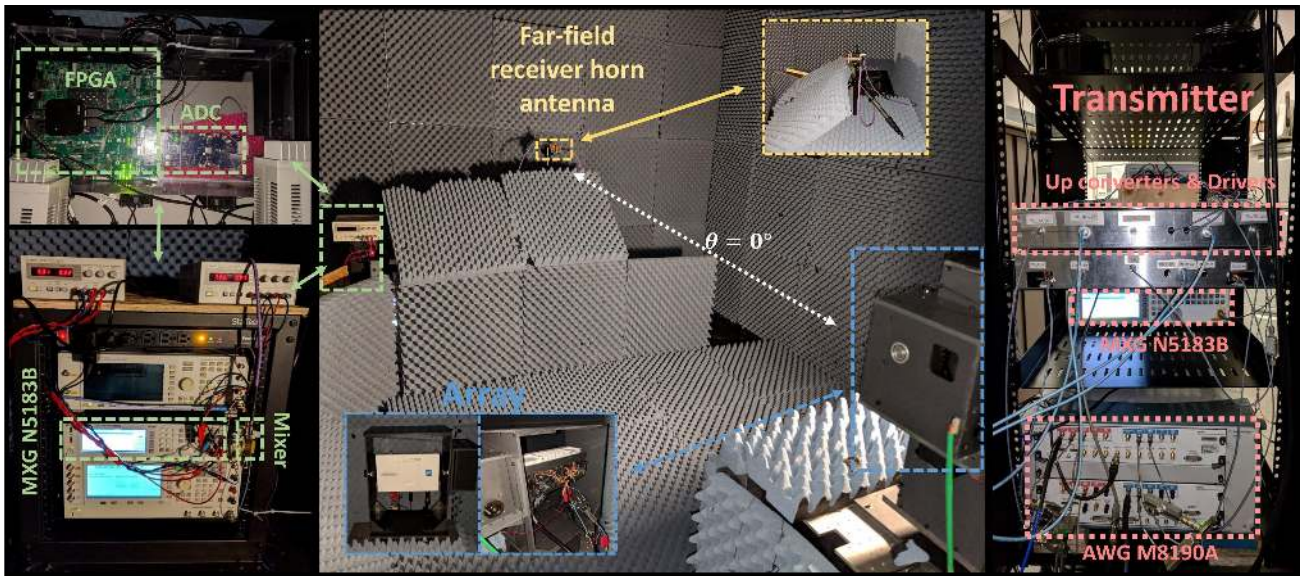

FIGURE 4. Photograph of measurement setup.

Moreover, since $C_{\tilde{x}_k\tilde{x}_k}(\tau + t_d^k)$ takes its maximum for $\tau + t_d^k = 0$ and decays quickly for $|\tau + t_d^k| > 0$, $C_{\tilde{x}_k\tilde{z}}(\tau)$ is small for $\tau \neq -t_d^k$. The time delay ,t_d^k, of the different RF chains can be estimated , from (14) as follows,

$$t_d^k = -\underset{\tau\in\mathbb{R}}{\text{argmax}}|C_{\tilde{x}_k\tilde{z}}(\tau)|. \tag{15}$$

and the relative phase-offsets with respect to ϕ_1, $\Delta\phi_k = \phi_k - \phi_1$, can be given by,

$$\Delta\phi_k = \angle C_{\tilde{x}_k\tilde{z}}(-t_d^k) - \angle C_{\tilde{x}_1\tilde{z}}(-t_d^1) \tag{16}$$

To determine the time delay t_d^k and the relative phase-offsets $\Delta\phi_k$ accurately, the cross-correlation in (13) is approximated by using an up-sampled discrete time cross-correlation function

$$C_{\tilde{x}_k\tilde{z}}[k] = \sum_{n=0}^{M'} \tilde{x}_k[n] \times \tilde{z}^*[n-k], \tag{17}$$

where M' is the length of the signals $\tilde{x}_k[n]$ and $\tilde{z}^*[n]$ after up-sampling. The up-sampling allows for fractional delay calibration and results in better cancellation of $x(t)$ in $y(t)$. The up-sampling ratio used in the following is $3 : 1$.

It is of note that while the derivation described above has been carried out for the LSMA front-ends in Fig. 1 (formed of two sub-arrays), it can be easily generalized for the case where the number of sub-arrays is greater than two, i.e. $K > 2$. In this case, the phase reference would be the MSA

This article has been accepted for publication in a future issue of this journal, but has not been fully edited. Content may change prior to final publication. Citation information: DOI 10.1109/ACCESS.2021.3096978, IEEE Access

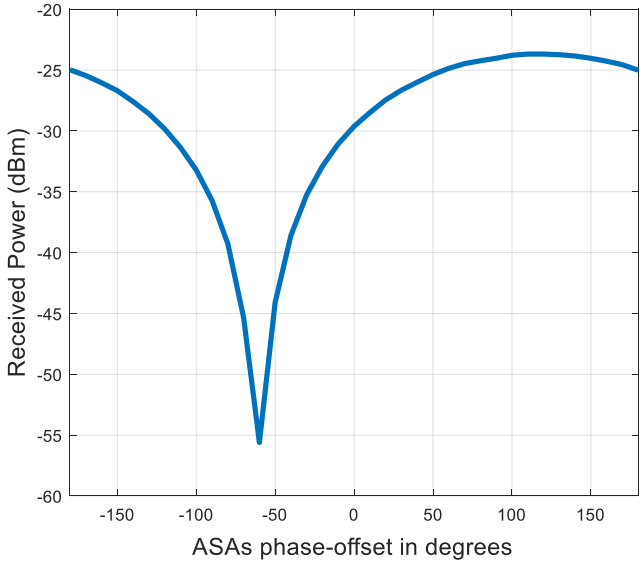

FIGURE 5. Received power at the TOR versus ASAs phase-offset with respect to the MSA.

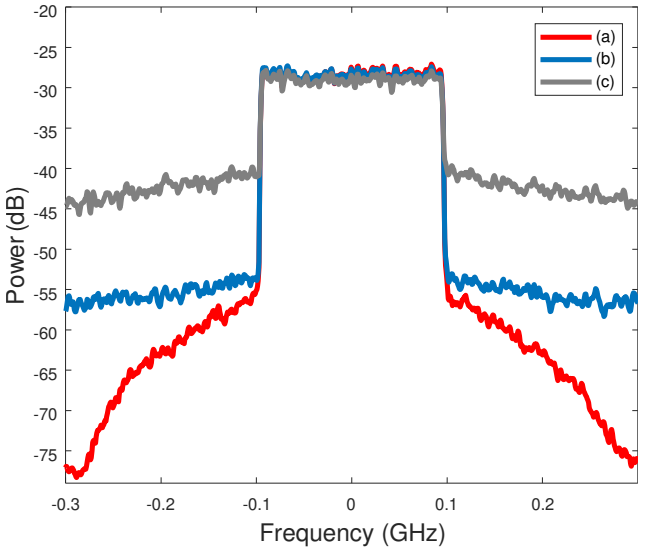

FIGURE 6. Far-field received signal for non-radiating ASAs without DPD using: (a) full 16-bit ADC resolution; (b) 4-bits ADC resolution; and (c) 2-bits ADC resolution.

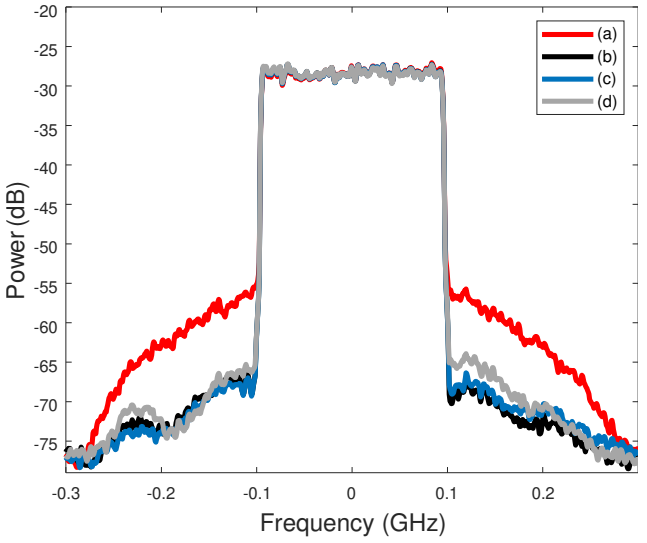

FIGURE 7. Far-field received signal spectrum (three ASAs case): (a) before DPD; (b) after DPD with non-radiating ASAs and 16-bit ADC; (c) after DPD with radiating ASAs and 4-bit ADC; and (d) after DPD with radiating ASAs and 2-bit ADC.

and finding the phase difference of each of the $(K-1)$ ASAs relative to a common MSA is the same procedure as determining the phase difference of one ASA relative to the MSA. Specifically, this procedure uses K uncorrelated signals to drive the $K-1$ ASAs and the MSA. It is to note that phase offsets do not change with DPD iteration since all the sub-arrays share the same LO signal. Moreover, delay and phase offset between the ASAs and the MSA in a hybrid beamforming system are expected to be a priori calibrated independently from the introduction of a DPD.

III. EXPERIMENTAL VALIDATION

A. MEASUREMENT SETUP

In order to demonstrate the capacity of the proposed DPD scheme (Fig. 1) to linearize an off-the-shelf mmwave hybrid-beamforming array, an experimental test bed was developed. The off-the-shelf hybrid beamforming array used for proof of concept validation in this work cannot be configured to realize the proposed DPD scheme in Fig. 1. Specifically, although it is designed for TDD transmission, the hardware cannot be setup to allow for the usage of the receiver modules as anti-beamforming during signal transmission by the sub-arrays. Furthermore, the high-level of the integration of the array under test does not allow the incorporation of the directional couplers and dedicated anti-beamforming receivers included in Fig. 1. Consequently, the combining step of $y(t)$ and $y_{aux}(t)$ in Fig. 1 was, instead, carried out in the far-field by combining the transmitted signals over-the-air and capturing the resulting error signal using a probing antenna.

The diagram shown in Fig. 3 depicts the measurement setup used to validate the proposed DPD system. The vector signal generation portion of the setup includes an arbitrary waveform generator (AWG, M8190A from Keysight Technologies) used to synthesize the test signals around an IF of 2.4 GHz. The IF signals are then up-converted to 28 GHz using an image-rejection IQ mixer (MMIQ1037H from Marki) and fed into an Anokiwave AWMF-0134 radio head [30] that includes the PAs, attenuators, phase shifters and four 64-element sub-arrays. Of the four sub-arrays, one was used as the MSA in this experiment and, depending on the experiment, two or three sub-arrays were used as ASAs. A receiving horn probing antenna was placed in the far-field and its output signal down-converted to IF using a down-converting mixer (MM11140H from Marki). The received IF signal was then digitized and used to train the DPD function. The radio head was attached to a step motor to automatically

This article has been accepted for publication in a future issue of this journal, but has not been fully edited. Content may change prior to final publication. Citation information: DOI 10.1109/ACCESS.2021.3096978, IEEE Access

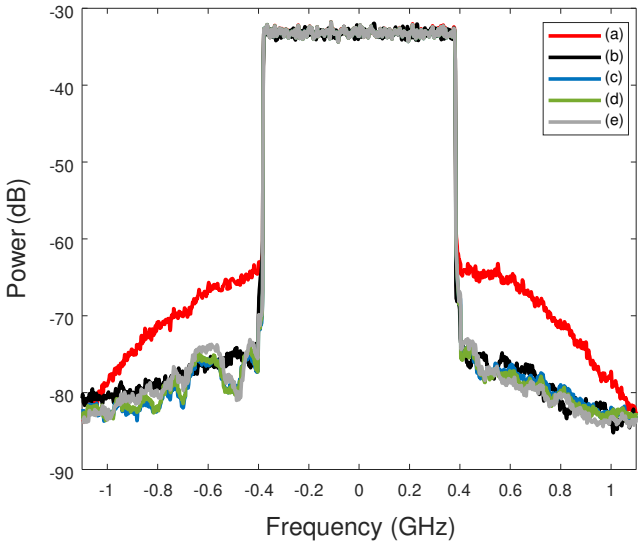

FIGURE 8. Far-field received signal spectrum (two-ASAs case): (a) before DPD; (b) after DPD with non-radiating ASAs and 16-bit ADC ; (c) after DPD with radiating ASAs and 16-bit ADC; (d) after DPD with radiating ASAs and 4-bit ADC; (e) after DPD with radiating ASAs and 2-bit ADC.

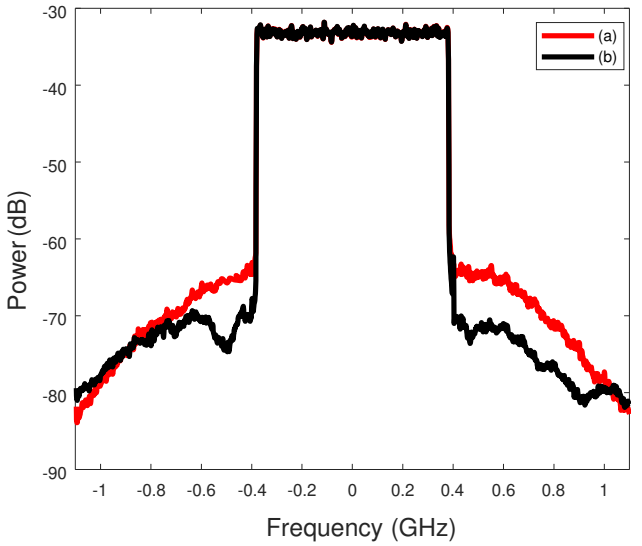

FIGURE 9. Far-field received signal spectrum (two-ASA case): (a) before DPD; (b) after DPD with radiating ASAs and 1-bit ADC.

control its relative angle to the receiving horn antenna.

The experiments were conducted using two wideband OFDM signals (200 MHz and 800 MHz bandwidth) with subcarriers modulated using 256-QAM, sub-carrier spacing of 120 KHz, and characterized by a PAPR of 10 dB. The test signals sampling rates were 1 Gsps and 4 Gsps respectively.

The setup shown in Fig. 4 was configured to allow for two experimental variations. Experiments used either two or three sub-arrays as ASAs that were operated at 6 dB and 9 dB backoff respectively. The MSA is setup to allow for a peak effective isotropic radiated power (EIRP) of $\cong 48$ dBm.

In the following, linearization capacity is assessed using the ACPR which is measured along the main beam direction before and after applying the DPD where the training is conducted using a TOR with a full as well as reduced (1, 2, and 4 bits) bit resolution ADC.

B. MEASUREMENT RESULTS USING THREE ASAS AND 200 MHZ TEST SIGNAL

In this variant, three sub-arrays were employed as ASAs and an OFDM signal with modulation bandwidth equal to 200 MHz was used as a test signal. The test signal was pre-processed to pre-compensate for the channel impulse response (channel between the MSA and the probing antenna), and then fed as the RF input of the MSA (64-element) of the four 64-element radio head. The same test signal was also pre-processed to account for the LO phase-offset, time misalignment and channel impulse response (channel between the three ASAs and the probing antenna) before driving the three remaining sub-arrays. The resulting error signal captured by the far-field probing antenna was then used to identify the coefficients of the CRV-series based SISO DPD function. For this, the nonlinearity order, nonlinear memory depth and linear memory depth were set to 5, 7 and 15 respectively, resulting in a total of 24 coefficients. The number of iterations used to train the DPD function was fixed to 10 iterations, $15,000$ samples were used per iteration and the step size was selected to be $\gamma_k = 1 - (k-1)/10$ for $k = 1, ..., 10$. Furthermore, the error signal was captured using an ADC (AD9208 from Analog Devices) with a sampling rate of 3 Gsps and 16-bit, 4-bit and 2-bit, and an analog bandwidth of 1.5 GHz.

Fig. 5 shows the measurement results of the received power of the modulated signals after over-the-air combining at the far-field receiver, versus different phase offsets between the MSA (to be linearized) and the ASAs. The point with the lowest received power corresponds where the phase offset between the MSA and ASA is calibrated. Fig. 5 is used to assess the sensitivity to phase calibration, i.e., how phase error can affect the cancellation of $y_{aux}(t) = x(t)$ from $f_{MSA}(x_{PD}(t)) = y(t)$ required to generate the error signal for DPD training and reduce the dynamic range of the received sampled signal. It is to note that as long as the phase offset between the MSA and ASAs is fixed, the DPD trained using direct learning yields excellent linearization performance. However, if the phase offset between the ASAs and the MSA is not accounted for, the dynamic range of the received signal and consequently, the ADC resolution cannot be reduced. Based on Fig. 5, it is also evident that the when the phase-offset is calibrated, the received power at the far-field receiver is about 30 dB less than the maximum. This is particularly interesting as it indicates that an ASA will reduce the required dynamic range at the TOR by almost 30 dB; hence, significantly reducing the required bit-depth of the TOR ADC.

Fig. 6, illustrates the measured spectrum without DPD and with non-radiating ASAs. From Fig. 6, it is clear that the

This article has been accepted for publication in a future issue of this journal, but has not been fully edited. Content may change prior to final publication. Citation information: DOI 10.1109/ACCESS.2021.3096978, IEEE Access

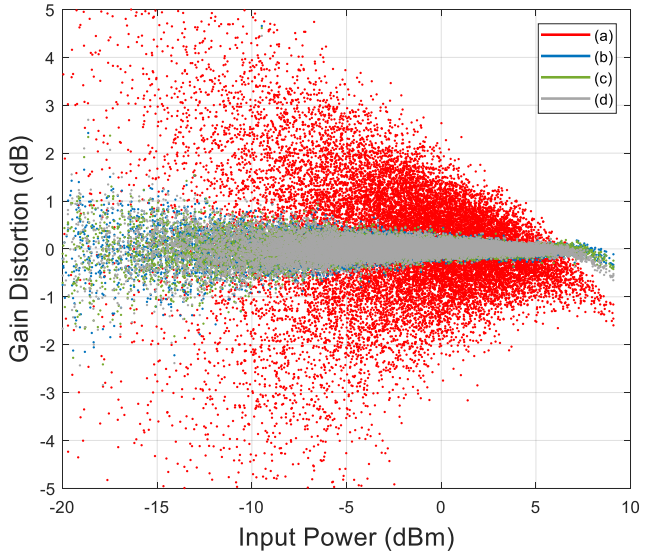

FIGURE 10. Far-field received signal gain distortion (two-ASAs case): a) before DPD; (b) after DPD with non-radiating ASAs and an 8-bits ADC; (c) after DPD with radiating ASAs and an 8-bits ADC; (d) after DPD with radiating ASAs and 4-bit ADC; (e) after DPD with radiating ASAs and 2-bit ADC.

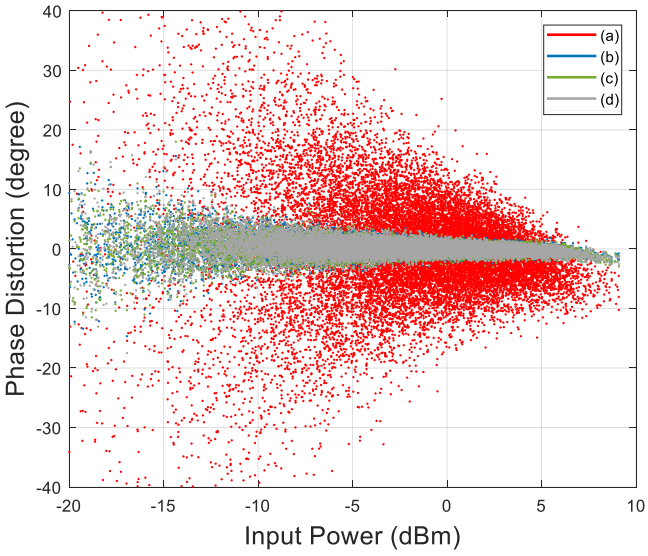

FIGURE 11. Far-field received signal phase distortion (two-ASAs case): a) before DPD; (b) after DPD with non-radiating ASAs and an 8-bits ADC; (c) after DPD with radiating ASAs and an 8-bit ADC; (d) after DPD with radiating ASAs and 4-bit ADC; (e) after DPD with radiating ASAs and 2-bit ADC.

cases using 4-bit and 2-bit ADC resolution imply a quantization noise in excess of the out-of-band distortion levels. Thus, for non-radiating ASAs, this limit the ability of the resulting DPD to demonstrate any appreciable linearization. These problems were not encountered when the DPD was trained using a 16-bit resolution ADC as can be seen in Fig. 7-(b). When the ASAs were used during the DPD training (as can be deduced from Fig. 7), a 4-bit resolution ADC allowed for a reduction in the adjacent channel power ratio (ACPR) from -33 to -43 dBc, and the error vector magnitude (EVM) dropped from 5.8% to 1.64%. These results are comparable to the DPD performance with non-radiating ASAs when using a full resolution receiver where ACPR and EVM after DPD were reduced to -42.3 dBc and 1.68% respective. According to Fig. 7-(d), when a 2-bit ADC is used during DPD training, linearization capacity was slightly reduced. The results in Fig. 7-(d) show an improvement in ACPR from -33 to -41.8 dBc and reduction in EVM from 5.8% to 2.1%.

C. MEASUREMENT RESULTS USING TWO ASAS AND 800 MHZ TEST SIGNAL

In this variant, two sub-arrays are employed as ASAs and an OFDM signal with modulation bandwidth equal to 800 MHz was used as a test signal. Again, as in the first variant, the error signal captured by the far-field probing antenna was used to identify the coefficients of the CRV-series based SISO DPD function. For this, the nonlinearity order, nonlinear memory depth and linear memory depth were set to 7, 9 and 0, respectively, resulting in a total of 13 coefficients. The DPD training was conducted using the same parameters (number of iterations, number of samples, and step size) as used in sub-section III-B. Note that during DPD training, the main beam was directed towards the broadside and the error signal was captured using a high-speed oscilloscope (DSA91304A from Keysight Technologies) with resolution of 8-bit, 4-bit, 3-bit, 2-bit and 1-bit, analog bandwidth of 13 GHz, and sampling rate of 40 Gsps.

Fig. 8 shows the spectrum captured at the far-field probing antenna: (a) before DPD; (b) after DPD with non-radiating ASAs and an 8-bit ADC; (c) after DPD with radiating ASAs and an 8-bit ADC; (d) after DPD with radiating ASAs and 4-bit ADC; (e) after DPD with radiating ASAs and 2-bit ADC. Based on Fig. 8, the application of the trained DPD in (c) with radiating ASAs and an 8-bit receiver allowed for a reduction of the ACPR and the EVM from -35 to -44 dBc and from 5.0% to 1.6%, respectively. These results were then compared to those obtained when the DPD was trained with non-radiating ASAs and using an 8-bit receiver where the ACPR was reduced from -35 to -43 dBc, and the EVM from 5.0% to 1.7%.

It is worth noting that the significant linearization capacity seen in Fig. 8 was obtained with different digitizer resolutions (i.e. full or 8-bit, 4-bit and 2-bit resolutions) and the EVM was maintained at 1.6%. This confirms that the ADC resolution reduction enabled by the proposed DPD scheme did not compromise the scheme's linearization capacity. The gain distortion and the AM-PM results at the far-field probing antenna are shown in Fig. 10 and Fig. 11 for: (a) before DPD; (b) after DPD with non-radiating ASAs and an 8-bit ADC; (c) after DPD with radiating ASAs and an 8-bit ADC; (d) after DPD with radiating ASAs and 4-bit ADC; (e) after DPD with radiating ASAs and 2-bit ADC.

A 1-bit receiver was also tested and the linearization performance is depicted in Fig. 9. Results show that even a

1-bit receiver resolution was able to improve the ACPR by approximately 5 dB and decrease the EVM by half, from 5% to 2.5%. As with the first set of measurement results, it was shown that better results could be achieved by increasing the number of training iterations.

IV. CONCLUSION

In this paper, a novel approach was proposed to reduce the TOR ADC bit resolution required to train a SISO DPD and linearize hybrid-beamforming arrays. This approach relies on an ASA anti-beamformer output to generate an inverted version of the input signal to the MSA – the sub-array to be linearized. The ASA and MSA anti-beamforming modules outputs are then combined to generate the error signal needed to train the DPD function. The digitization of the resulting error signal then requires an ADC with a few bits of resolution. Experimental validation of the proposed DPD scheme showed excellent linearization capacity with only 4 or 2-bit resolution ADC when applied to an array comprised of four 64-element sub-arrays operating at 28 GHz. The attained linearization capacity was comparable to the one achieved with a 16 bit resolution ADC.

REFERENCES

[1] K. Hausmair, S. Gustafsson, C. Sánchez-Pérez, P. N. Landin, U. Gustavsson, T. Eriksson, and C. Fager, "Prediction of Nonlinear Distortion in Wideband Active Antenna Arrays," IEEE Transactions on Microwave Theory and Techniques, vol. 65, no. 11, pp. 4550–4563, 2017.

[2] K. Hausmair, P. N. Landin, U. Gustavsson, C. Fager, and T. Eriksson, "Digital Predistortion for Multi-Antenna Transmitters Affected by Antenna Crosstalk," IEEE Transactions on Microwave Theory and Techniques, vol. 66, no. 3, pp. 1524–1535, 2018.

[3] G. Zakka El Nashef, F. Torres, S. Mons, T. Reveyrand, T. Monediere, E. Ngoya, and R. Quere, "EM/Circuit Mixed Simulation Technique for an Active Antenna," IEEE Antennas and Wireless Propagation Letters, vol. 10, pp. 354–357, 2011.

[4] F. M. Barradas, P. M. Tomé, J. M. Gomes, T. R. Cunha, P. M. Cabral, and J. C. Pedro, "Power, Linearity, and Efficiency Prediction for MIMO Arrays With Antenna Coupling," IEEE Transactions on Microwave Theory and Techniques, vol. 65, no. 12, pp. 5284–5297, 2017.

[5] S. Lee, M. Kim, Y. Sirl, E. Jeong, S. Hong, S. Kim, and Y. H. Lee, "Digital Predistortion for Power Amplifiers in Hybrid MIMO Systems with Antenna Subarrays," in 2015 IEEE 81st Vehicular Technology Conference (VTC Spring), 2015, pp. 1–5.

[6] H. Yan and D. Cabric, "Digital Predistortion for Hybrid Precoding Architecture in Millimeter-Wave Massive MIMO Systems," in 2017 IEEE International Conference on Acoustics, Speech and Signal Processing (ICASSP), 2017, pp. 3479–3483.

[7] N. Tervo, J. Aikio, T. Tuovinen, T. Rahkonen, and A. Parssinen, "Digital Predistortion of Amplitude Varying Phased Array Utilising Over-The-Air Combining," in 2017 IEEE MTT-S International Microwave Symposium (IMS), 2017, pp. 1165–1168.

[8] L. Liu, W. Chen, L. Ma, and H. Sun, "Single-PA-Feedback Digital Predistortion for Beamforming MIMO Transmitter," in 2016 IEEE International Conference on Microwave and Millimeter Wave Technology (ICMMT), vol. 2, 2016, pp. 573–575.

[9] A. Brihuega, L. Anttila, M. Abdelaziz, T. Eriksson, F. Tufvesson, and M. Valkama, "Digital Predistortion for Multiuser Hybrid MIMO at MmWaves," IEEE Transactions on Signal Processing, vol. 68, pp. 3603–3618, 2020.

[10] X. Liu, Q. Zhang, W. Chen, H. Feng, L. Chen, F. M. Ghannouchi, and Z. Feng, "Beam-Oriented Digital Predistortion for 5G Massive MIMO Hybrid Beamforming Transmitters," IEEE Transactions on Microwave Theory and Techniques, vol. 66, no. 7, pp. 3419–3432, 2018.

[11] M. Abdelaziz, L. Anttila, A. Brihuega, F. Tufvesson, and M. Valkama, "Digital Predistortion for Hybrid MIMO Transmitters," IEEE Journal of Selected Topics in Signal Processing, vol. 12, no. 3, pp. 445–454, 2018.

[12] E. Ng, Y. Beltagy, P. Mitran, and S. Boumaiza, "Single-Input Single-Output Digital Predistortion of Power Amplifier Arrays in Millimeter Wave RF Beamforming Transmitters," in 2018 IEEE/MTT-S International Microwave Symposium - IMS, 2018, pp. 481–484.

[13] A. Brihuega, M. Abdelaziz, L. Anttila, M. Turunen, M. Allén, T. Eriksson, and M. Valkama, "Piecewise Digital Predistortion for MmWave Active Antenna Arrays: Algorithms and Measurements," IEEE Transactions on Microwave Theory and Techniques, vol. 68, no. 9, pp. 4000–4017, 2020.

[14] X. Liu, W. Chen, L. Chen, F. M. Ghannouchi, and Z. Feng, "Linearization for Hybrid Beamforming Array Utilizing Embedded Over-the-Air Diversity Feedbacks," IEEE Transactions on Microwave Theory and Techniques, vol. 67, no. 12, pp. 5235–5248, 2019.

[15] A. B. Ayed, G. Scarlato, P. Mitran, and S. Boumaiza, "On the Effectiveness of Near-Field Feedback for Digital Pre-Distortion of Millimeter-Wave RF Beamforming Arrays," in 2020 IEEE/MTT-S International Microwave Symposium (IMS), 2020, pp. 547–550.

[16] Y. Cao, A. B. Ayed, J. Xia, and S. Boumaiza, "Uniformly Distributed Near-Field Probing Array for Enhancing the Performance of 5G Millimetre-wave Beamforming Transmitters," IEEE Microwave and Wireless Components Letters, pp. 1–1, 2021.

[17] C. Yu, J. Jing, H. Shao, Z. H. Jiang, P. Yan, X. Zhu, W. Hong, and A. Zhu, "Full-Angle Digital Predistortion of 5G Millimeter-Wave Massive MIMO Transmitters," IEEE Transactions on Microwave Theory and Techniques, vol. 67, no. 7, pp. 2847–2860, 2019.

[18] C. Yu, L. Guan, E. Zhu, and A. Zhu, "Band-Limited Volterra Series-Based Digital Predistortion for Wideband RF Power Amplifiers," IEEE Transactions on Microwave Theory and Techniques, vol. 60, no. 12, pp. 4198–4208, 2012.

[19] Y. Li, J. Zhai, C. Yu, Z. Jiang, and L. Zhang, "A Band-Limited CPWL-Based Memory Polynomial Model for Digital Predistortion," in 2017 Sixth Asia-Pacific Conference on Antennas and Propagation (APCAP), 2017, pp. 1–3.

[20] Y. Liu, J. J. Yan, H. Dabag, and P. M. Asbeck, "Novel Technique for Wideband Digital Predistortion of Power Amplifiers With an Under-Sampling ADC," IEEE Transactions on Microwave Theory and Techniques, vol. 62, no. 11, pp. 2604–2617, 2014.

[21] Y. Beltagy, P. Mitran, and S. Boumaiza, "Direct Learning Algorithm for Digital Predistortion Training Using Sub-Nyquist Intermediate Frequency Feedback Signal," IEEE Transactions on Microwave Theory and Techniques, vol. 67, no. 1, pp. 267–277, 2019.

[22] Y. Liu, C. Huang, X. Quan, P. Roblin, W. Pan, and Y. Tang, "Novel Linearization Architecture with Limited ADC Dynamic Range for Green Power Amplifiers," IEEE Journal on Selected Areas in Communications, vol. 34, no. 12, pp. 3902–3914, 2016.

[23] H. Wang, G. Li, C. Zhou, W. Tao, F. Liu, and A. Zhu, "1-bit Observation for Direct-Learning-Based Digital Predistortion of RF Power Amplifiers," IEEE Transactions on Microwave Theory and Techniques, vol. 65, no. 7, pp. 2465–2475, 2017.

[24] N. Tervo, J. Aikio, T. Tuovinen, T. Rahkonen, and A. Parssinen, "Digital Predistortion of Amplitude Varying Phased Array Utilising Over-The-Air Combining," in 2017 IEEE MTT-S International Microwave Symposium (IMS), 2017, pp. 1165–1168.

[25] X. Liu, Q. Zhang, W. Chen, H. Feng, L. Chen, F. M. Ghannouchi, and Z. Feng, "Beam-Oriented Digital Predistortion for 5G Massive MIMO Hybrid Beamforming Transmitters," IEEE Transactions on Microwave Theory and Techniques, vol. 66, no. 7, pp. 3419–3432, 2018.

[26] F. Mkadem, M. C. Fares, S. Boumaiza, and J. Wood, "Complexity-Reduced Volterra Series Model for Power Amplifier Digital Predistortion," Analog Integrated Circuits and Signal Processing, vol. 79, no. 2, pp. 331–343, 2014.

[27] A. Chung, A. M. Darwish, E. Viveiros, H. A. Hung, P. Mitran, and S. Boumaiza, "Analysis and Compensation of Nonidealities in Frequency Multiplier-Based High-Frequency Vector Signal Generators," IEEE Transactions on Microwave Theory and Techniques, vol. 67, no. 6, pp. 2270–2283, 2019.

[28] R. N. Braithwaite, "Memory Correction of a Doherty Power Amplifier with a WCDMA Input using Digital Predistortion," in IEEE MTT-S Int. Microw. Symp. Dig., Jun. 2006, pp. 1526–1529.

[29] C. Knapp and G. Carter, "The generalized correlation method for estimation of time delay," IEEE Transactions on Acoustics, Speech, and Signal Processing, vol. 24, no. 4, pp. 320–327, 1976.

[30] "AWA-0134." [Online]. Available: https://www.anokiwave.com/products/awa-0134/index.html

AHMED BEN AYED (S'18) received the B.Sc. degree from the Hong Kong University of Science and Technology, Hong Kong, in 2017 and his M.A.Sc. degree from the University of Waterloo, Canada, in 2019. He is currently pursuing his Ph.D. degree in electrical and computer engineering at the University of Waterloo EmRG Lab. His main research interests are in the area of millimeter-wave communication systems, signal processing, nonlinear system modeling and linearization techniques.

ERIC NG (S'14-M'18)) received the bachelor's degree in electrical engineering and the master's degree in electrical and computer engineering from the University of Waterloo, Waterloo, ON, Canada, in 2016 and 2018, respectively. From 2014 to 2018, he was with the Emerging Radio Systems Group, where he was involved in digitally assisted linearization techniques for power-efficient RF and millimeter-wave communications systems. He is currently with Anokiwave, Billerica, MA, USA, where he is involved in active phased-array system design and performance optimization for 5G and sat-com applications.

PATRICK MITRAN (S'01-M'07-SM'13) received the bachelor's and master's degrees in electrical engineering from McGill University, Montreal, QC, Canada, in 2001 and 2002, respectively, and the Ph.D. degree from the School of Engineering and Applied Sciences, Harvard University, Cambridge, MA, USA, in 2006. In 2005, he was a Research Scientist with the Radio Communications Laboratory, Intel Corporation. From 2006 to 2007, he was a Lecturer in applied mathematics with the School of Engineering and Applied Sciences, Harvard University. He is currently a Professor with the Department of Electrical and Computer Engineering, University of Waterloo, Waterloo, ON, Canada. His current research interests include information theory and wireless communications, as well as cross-layer design and signal processing for 5G. Dr. Mitran was the recipient of the Government of Ontario Early Researcher Award in 2011. He is a licensed Professional Engineer in the Province of Ontario. From 2012 to 2016, he served as an Editor for the IEEE TRANSACTIONS ON COMMUNICATIONS and from 2016 to 2019 he served as an Associate Editor for the IEEE TRANSACTIONS ON INFORMATION THEORY.

SLIM BOUMAIZA (S'00-M'04-SM'07) received the B.Eng. degree in electrical engineering from the École Nationale d'ingénieurs de Tunis, Tunis, Tunisia, in 1997, and the M.S. and Ph.D. degrees from the École Polytechnique de Montréal, Montreal, QC, Canada, in 1999 and 2004, respectively. He is currently a professor with the Department of Electrical and Computer Engineering, University of Waterloo, where he leads the Emerging Radio System Research Group. He has extensive experience in the development of high performance (energy-efficient, linear) wireless transmitters for 3G/4G/5G radio systems. This includes expertise in the characterization, modeling, and design of microwave circuits, high efficiency power amplifier design and linearization techniques, and mixed RF/digital signal processing design methodology. A recipient of an Early Researcher Award from the Ontario Research Fund, and NSERC Accelerator and Synergy awards, his work has been published in 70 journal articles and over 120 conference papers.